Acta Crystallographica Section F
Structural Biology and Crystallization Communications
ISSN 1744-3091

Structure of *Physarum polycephalum* cytochrome b_5 reductase at 1.56 Å resolution

Sangwoo Kim,[a] Michihiro Suga,[a] Kyoko Ogasahara,[a] Terumi Ikegami,[b] Yoshiko Minami,[b] Toshitsugu Yubisui[b] and Tomitake Tsukihara[a]*

[a]Institute for Protein Research, Osaka University, 3-2 Yamada-oka, Suita, Osaka, Japan, and [b]Department of Biochemistry, Okayama University of Science, 1-1 Ridai-cho, Okayama 700-0005, Japan

Correspondence e-mail: tsuki@protein.osaka-u.ac.jp

Received 22 January 2007
Accepted 7 March 2007

PDB Reference: *P. polycephalum* cytochrome b_5 reductase, 2eix, r12eixsf.

Physarum polycephalum cytochrome b_5 reductase catalyzes the reduction of cytochrome b_5 by NADH. The structure of *P. polycephalum* cytochrome b_5 reductase was determined at a resolution of 1.56 Å. The molecular structure was compared with that of human cytochrome b_5 reductase, which had previously been determined at 1.75 Å resolution [Bando *et al.* (2004), *Acta Cryst.* D**60**, 1929–1934]. The high-resolution structure revealed conformational differences between the two enzymes in the adenosine moiety of the FAD, the lid region and the linker region. The structural properties of both proteins were inspected in terms of hydrogen bonding, ion pairs, accessible surface area and cavity volume. The differences in these structural properties between the two proteins were consistent with estimates of their thermostabilities obtained from differential scanning calorimetry data.

1. Introduction

Cytochrome b_5 reductase (cyt b_5R; EC 1.6.2.2), which is involved in the microsomal electron-transport system and erythrocyte function, catalyzes the two-electron transfer from NADH through FAD (flavin adenine dinucleotide; Strittmatter, 1965; Iyanagi *et al.*, 1984) to two molecules of cytochrome b_5.

This enzyme is known to exist in two forms: a membrane-bound form and a soluble form. The membrane-bound form is composed of a hydrophobic domain (residues 1–25, MW $\simeq$ 3 kDa) and a catalytic domain (residues 26–300, MW $\simeq$ 30 kDa). The hydrophobic domain serves to anchor the protein to the microsome *via* strong noncovalent interactions with the lipid bilayer. The catalytic domain, which contains an active site and FAD, projects into the surrounding cytosol. This form is primarily embedded in the endoplasmic reticulum membrane as an amphipathic protein and participates in a variety of metabolic transformations, such as the desaturation (Oshino *et al.*, 1971) and elongation of fatty acids (Keyes & Cinti, 1980), cholesterol biosynthesis (Reddy *et al.*, 1977) and cytochrome P450-dependent hydroxylation reactions (Hildebrandt & Estabrook, 1971). The soluble form, which only contains the catalytic domain, is found in circulating erythrocytes, where it catalyzes methaemoglobin reduction in the electron-transport system (Hultquist & Passon, 1971).

Cyt b_5R proteins have been identified in a wide range of eukaryotic genomes, including those of fungi (Csukai *et al.*, 1994), yeast (GenBank CAA86908), plants (Fukuchi-Mizutani *et al.*, 1999), nematodes (Kamath *et al.*, 2003), insects (Jones *et al.*, 2001), fish (GenBank BC045880), amphibians (Klein *et al.*, 2002), birds (GenBank AJ294706) and mammals (Strittmatter, 1965; Yubisui *et al.*, 1986). The structures of soluble cyt b_5R proteins from pig (Nishida, Inaka & Miki, 1995; Nishida, Inaka, Yamanaki *et al.*, 1995), rat (Bewley *et al.*, 2001) and human (Bando *et al.*, 2004) have been determined using X-ray crystallography.

The slime mould *Physarum polycephalum*, a member of the myxomycetes, has a life cycle that includes a characteristic plasmodium phase during which the mould contains many nuclei but is not subdivided into cells. To grow, *P. polycephalum* has an unusual and

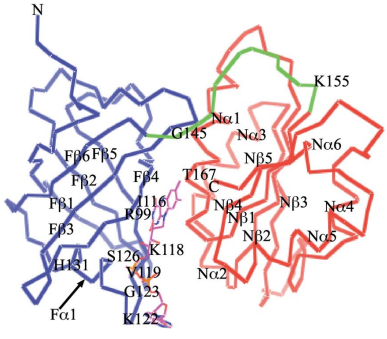

© 2007 International Union of Crystallography
All rights reserved

Table 1
Intensity data and structural refinement statistics.

Values in parentheses are for the outer shell.

Intensity data	
Space group	$P2_12_12_1$
Unit-cell parameters	
a (Å)	101.08
b (Å)	136.37
c (Å)	45.72
Resolution range (Å)	43.355–1.56 (1.62–1.56)
Total No. of reflections	622056
No. of unique reflections	88222
Completeness (%)	97.7 (93.9)
R_{merge} (%)	8.0 (41.1)
$I/\sigma(I)$	28.5 (3.7)
Redundancy	7.1
Refinement	
No. of working reflections	83782
No. of free reflections	4185
R factor (%)	18.4
R_{free} (%)	22.6
R.m.s.d. bond lengths (Å)†	0.02
R.m.s.d. bond angles (°)†	2.0
No. of protein atoms	3900
No. of water molecules	474

† Root-mean-square deviations from ideal structure.

specific requirement for protohaem. This requirement can be used when studying the mechanism and regulation of the mitochondrial electron-transport chain. Here, the structure of *P. polycephalum* cyt b_5R was determined at 1.56 Å resolution in a study aimed at understanding the role of cyt b_5R in the unique life cycle of the organism. By comparing the structure with that of human cyt b_5R in terms of the three-dimensional architecture and the thermal phase transition, we have examined the relationship between the structure and thermal stability of this enzyme.

2. Materials and methods

2.1. Crystallization

Cyt b_5R from *P. polycephalum* was expressed as described previously (Shirabe *et al.*, 1989; Ikegami *et al.*, 2007). The enzyme was overexpressed in *Escherichia coli* as an α-thrombin-cleavable fusion protein. The protein, which lacked the 33 N-terminal amino-acid residues, was then purified and used in crystallization experiments.

Crystals of *P. polycephalum* cyt b_5R were grown using the hanging-drop vapour-diffusion method (McPherson, 1999). A 1.5 µl drop of 0.7%(*w*/*v*) protein solution (pH 7.0) was equilibrated against 1.5 µl 50 m*M* *n*-(2-acetamido)iminodiacetic acid buffer pH 7.0 containing 200 m*M* NaI and 18–20% PEG 4000 at 293 K. A crystal (0.6 × 0.08 × 0.1 mm) was transferred into reservoir solution containing 25% glycerol as a cryoprotectant before collection of diffraction data.

2.2. Diffraction data collection and structure determination

Diffraction data were collected at 100 K at the BL44XU beamline of SPring-8, which was equipped with a DIP6040 image-plate detector. Diffraction images were processed and scaled with *DENZO* and *SCALEPACK* (Otwinowski & Minor, 1997), respectively.

The crystal belonged to the orthorhombic space group $P2_12_12_1$, with unit-cell parameters $a = 101.08$, $b = 136.37$, $c = 45.72$ Å. The value of the Matthews coefficient was 2.49 Å^3 Da^{-1} for one molecule per asymmetric unit, which corresponded to a solvent content of 50.7%.

The structure was determined using the molecular-replacement method (Rossmann & Blow, 1962) and the atomic parameters of human cyt b_5R (PDB code 1umk; Bando *et al.*, 2004). *MOLREP* was used for molecular replacement. The electron-density map was calculated with *SFALL* and *SIGMAA* from the *CCP*4 program suite (Collaborative Computational Project, Number 4, 1994). The structural model was manipulated using *Coot* (Emsley & Cowtan, 2004) and was refined with *REFMAC*5 (Murshudov *et al.*, 1997) and *CNS* (Brünger *et al.*, 1998). Solvent molecules were automatically added using *ARP*/*wARP* during the refinement cycles. The model was fitted to the composite OMIT map and the FAD molecule was built into the electron-density map. Structural refinement was performed until the model could not be improved as judged by a reduction in the R_{free} value. The statistics of the refinement are summarized in Table 1. The stereochemical quality of the refined structure was inspected using *PROCHECK* (Laskowski *et al.*, 1993). In the structure, 96.1% of the nonglycine residues were in the most favourable regions of the Ramachandran plot; the remaining eight residues were in additional allowed regions and no residues were in disallowed regions. The overall *G* factor was −0.1.

2.3. Differential scanning calorimetry (DSC)

DSC was carried out with a MicroCal VP-DSC differential scanning calorimeter (Northampton, MA, USA). Prior to measurements, the protein solutions were dialyzed against 10 m*M* sodium phosphate buffer pH 7.6. The dialyzed samples were filtered through a 0.22 µm pore-size membrane and then degassed in a vacuum. The DSC thermograms were obtained at a scan rate of 1 K min^{-1} with a protein concentration of 1.1–1.4 mg ml^{-1}. The DSC curves were analyzed

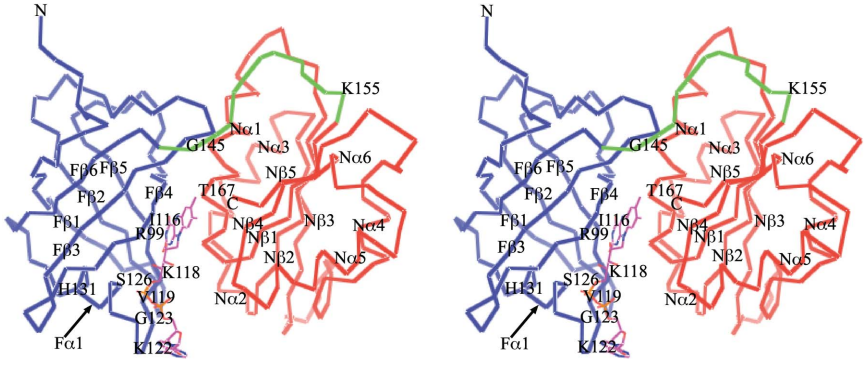

Figure 1
Stereoview of *P. polycephalum* cyt b_5R. The subdomains include the FAD-binding domain (blue), the NADH-binding domain (red) and the linker region (green). The FAD molecule is shown as a stick model. Amino-acid residues are shown using the single-letter notation and the secondary structures marked in Fig. 2 are shown. The capital letters N and C represent the amino- and carboxy-termini, respectively. This figure was produced using *PyMOL*.

using *Origin* software from MicroCal for the curves, subtracting a thermogram of buffer alone obtained under identical conditions.

3. Results and discussion

3.1. *P. polycephalum* cyt b_5R structure

The three-dimensional structure of *P. polycephalum* cyt b_5R was determined at 1.56 Å resolution. The final model included one protein molecule containing 243 amino-acid residues (Lys39–Phe281), one FAD molecule, one glycerol molecule, two iodide ions, one sodium ion and 237 water molecules in each crystallographic asymmetric unit. The first five residues of the protein (Glu34–Ser38) were invisible in the electron-density maps.

As shown in Fig. 1, the structure consists of two major domains: the N-terminal FAD-binding domain (Lys39–His144) and the C-terminal NADH-binding domain (Glu156–Phe281). The FAD-binding domain is a β-barrel consisting of six antiparallel β-strands (Fβ1–Fβ6) with a Greek-key motif. An α-helix (Fα1; Gly123–His131) and a short loop (Val119–Lys122) are attached to the β-barrel (Fig. 2). The NADH-binding domain has three $\beta\alpha\beta$ motifs (Rossmann *et al.*, 1974, 1975). These domains are linked by the linker region (Gly145–Lys155), which is a random coil that may function as a hinge to allow efficient electron transfer of the reducing equivalents from the NADH molecule to the FAD molecule by correctly orienting the FAD- and NADH-binding domains (Bewley *et al.*, 2001; Davis *et al.*, 2004). The linker region is shorter than those of the cyt b_5R proteins from higher eukaryotes (Figs. 2 and 3*c*), including the cyt b_5R proteins from pig, rat and humans; these proteins have a larger 29-amino-acid linker region and three antiparallel β-strands are formed in the middle of the protein (Nishida, Inaka & Miki, 1995; Nishida, Inaka, Yamanaka *et al.*, 1995; Bewley *et al.*, 2001; Bando *et al.*, 2004). Phe147, Tyr149 and Lys155 of the linker region interact with Gln84 of the FAD-binding domain and Asn179 and Asp249 of the NADH-binding domain, respectively.

The 'lid region' (Val119–Lys122; Fig. 2), which forms a surface-exposed loop, is nine residues shorter than the corresponding region in human cyt b_5R (Fig. 3*a*). The protrusion of the lid from the Fα1 helix is smaller than that of human cyt b_5R by approximately 5 Å. Tyr120 O forms hydrogen bonds with Gly123 N and Gln127 $N^{\varepsilon 2}$; Tyr120 N also forms a hydrogen bond with Ser126 O^{γ}. These hydrogen bonds stabilize the loop structure of the lid.

The FAD molecule is located between the two domains, but primarily interacts with the FAD-binding domain. The flavin mononucleotide (FMN) moiety of *P. polycephalum* cyt b_5R can be superposed on that of the human cyt b_5R, whereas the adenine moieties of the two cyt b_5R proteins have different orientations (Fig. 3). The riboflavin ring moiety is located in a predominantly hydrophobic pocket, where it makes van der Waals interactions with the Fβ4 strand (residues 85–101) and the Nα1 helix (residues 163–178); Fβ4 contains part of the FAD-binding motif (R*x*YT*xx*S; residues 99–105) and Nα1 includes the NADH-binding motif (G*x*G*xx*P; residues 163–168). In addition to hydrophobic interactions, hydrogen bonds tightly fix the FAD molecule between the FAD- and the NADH-binding domains (Fig. 4), as has been observed in other cyt b_5R proteins (Nishida, Inaka & Miki, 1995; Nishida, Inaka, Yamanaka *et al.*, 1995; Bewley *et al.*, 2001; Bando *et al.*, 2004). N3, N5 and O2 of the riboflavin-ring moiety form a hydrogen bond with Ile116 O, Thr167 $O^{\gamma 1}$ and Lys118 N, respectively. The OP2 of the pyrophosphate moiety of FAD interacts with O^{γ} and N of Ser126. AO3 of the ribose forms a hydrogen bond with Lys122 N. Unlike human cyt b_5R, which has a hydrogen bond between AN6 of the adenine moiety and Phe113 N, the adenine moiety of *P. polycephalum* cyt b_5R did not form any hydrogen bonds to the protein. The interaction between the FMN

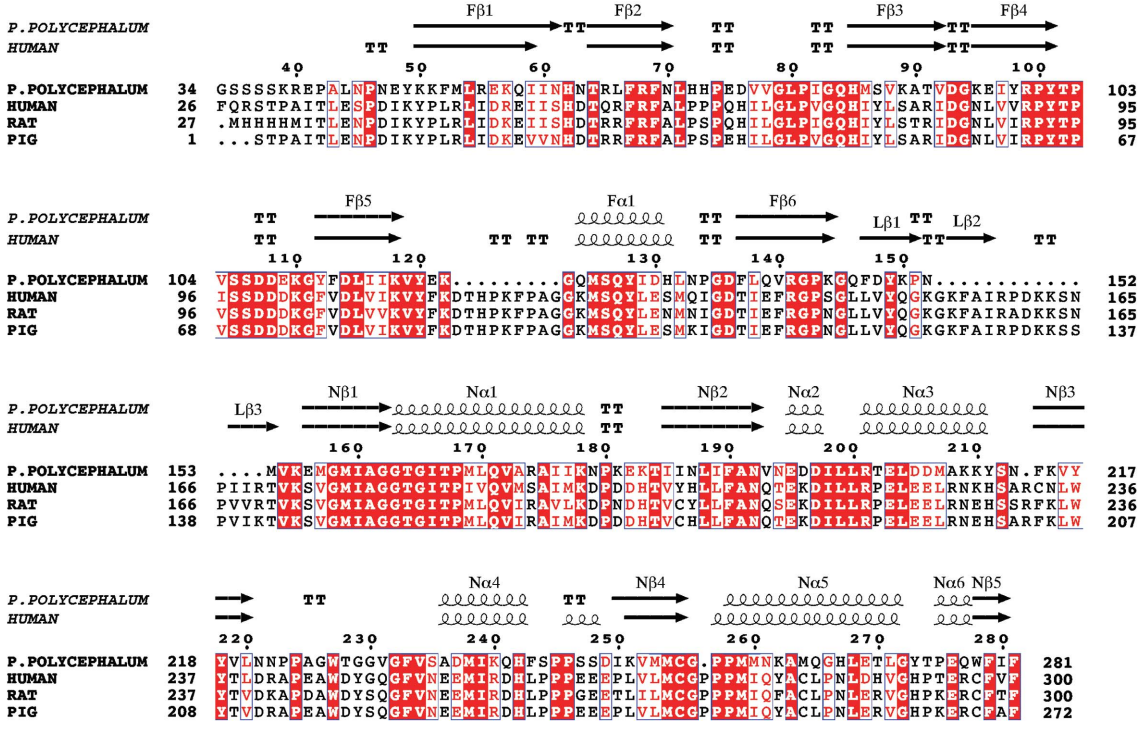

Figure 2
Sequence alignment of cyt b_5R proteins from *P. polycephalum*, human, rat and pig. The secondary-structure elements are marked on top of the alignment: α-helices by a helix, β-strands by an arrow and turns by the letters TT. Conserved residues are boxed in white on a red background; similar residues are boxed in red with a white background. This figure was produced using *ClustalW*.

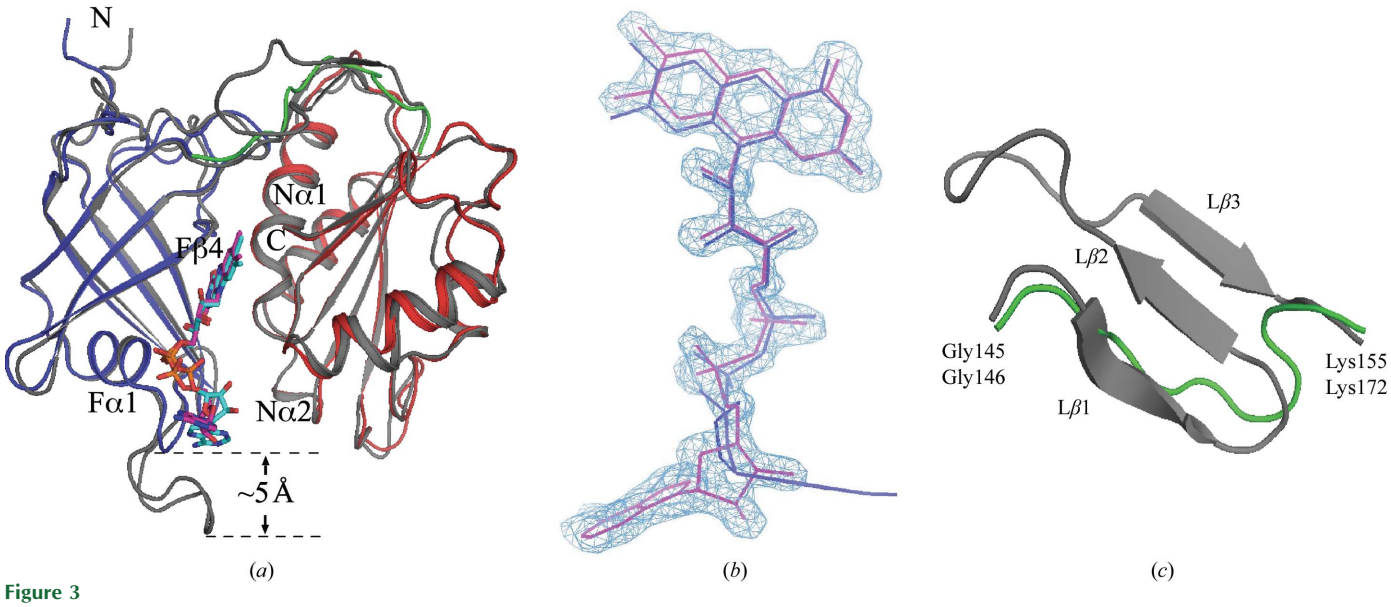

Figure 3
Comparison of the structures of the *P. polycephalum* and human cyt b_5R proteins. (*a*) Ribbon diagrams of the structures of the *P. polycephalum* and human cyt b_5R proteins. The *P. polycephalum* cyt b_5R subdomains are coloured as in Fig. 1. Secondary structure and amino- and carboxy-termini are represented as in Fig. 1. The structure of human cyt b_5R is shown in grey. The FAD is shown in pink in *P. polycephalum* cyt b_5R and in cyan in human cyt b_5R. (*b*) The FAD molecule of *P. polycephalum* cyt b_5R (pink) located in the $F_o - F_c$ electron density (blue cage). The FAD of human cyt b_5R, represented by a blue stick model, is superposed on the FAD of *P. polycephalum* cyt b_5R. (*c*) Ribbon diagrams of the structures of the *P. polycephalum* (green; Gly145–Lys155) and human (grey; Gly146–Lys172) cyt b_5R linker regions.

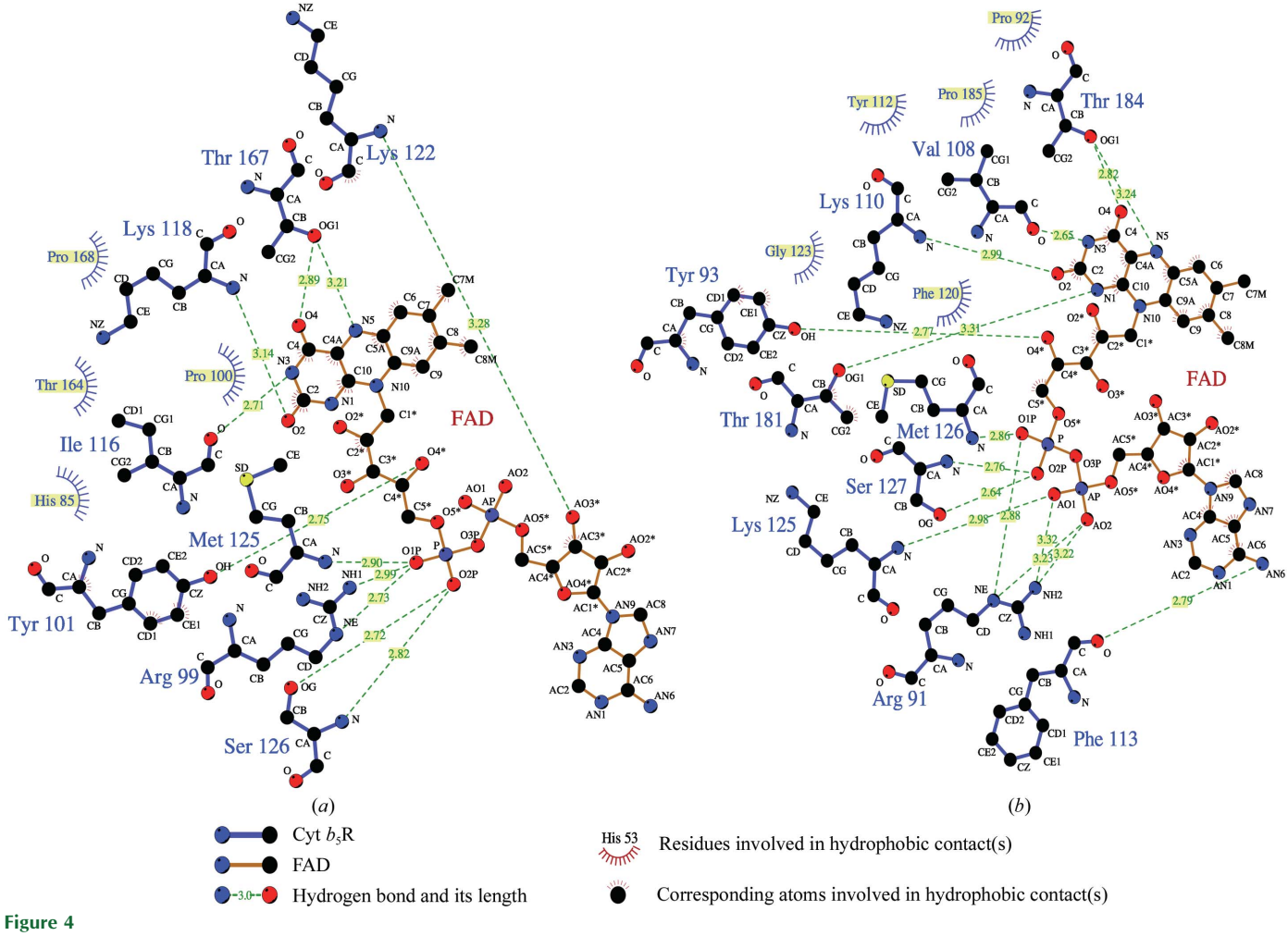

Figure 4
Comparison of the interactions between the enzymes and the FAD molecule. (*a*) The interaction between the FAD and *P. polycephalum* cyt b_5R. (*b*) The interaction between FAD and human cyt b_5R. Hydrogen bonds are shown as green dashed lines and van der Waals contacts are denoted as purple combs. This figure was produced using *LIGPLOT*.

Table 2
The amino-acid compositions of the *P. polycephalum* and human cyt b_5R proteins.

	P. polycephalum cyt b_5R		Human cyt b_5R	
Residue	No.	% of total residues	No.	% of total residues
Hydrophobic	124	51.0	143	52.0
Ala	10	4.1	12	4.4
Gly	19	7.8	19	6.9
Ile	18	7.4	22	8.0
Leu	16	6.6	25	9.1
Met	14	5.8	8	2.9
Phe	12	4.9	12	4.4
Pro	18	7.4	27	9.8
Trp	2	0.8	2	0.7
Val	15	6.2	16	5.8
Neutral	45	18.5	47	17.1
Asn	15	6.2	7	2.5
Cys	1	0.4	4	1.5
Gln	10	4.1	11	4.0
Ser	9	3.7	13	4.7
Thr	10	4.1	12	4.4
Hydrophilic	67	27.6	75	27.3
Arg	8	3.3	16	5.8
Asp	14	5.8	19	6.9
Glu	13	5.3	15	5.5
His	7	2.9	10	3.6
Lys	21	8.6	15	5.5
Tyr	11	4.5	10	3.6
Total No.	243		275	

moiety and the protein in *P. polycephalum* cyt b_5R was similar to that observed in human cyt b_5R.

To compare the structures of the *P. polycephalum* and human cyt b_5R proteins, the structures of the two enzymes were superposed using the least-squares method. The root-mean-square deviations for each C^{α} atom and for each side chain are given in Fig. 5. Although the overall structures clearly superposed with each other, local structural differences were detected in various regions, including Lys39–Asn45 (I), Ser106–Asp107 (II), Lys122 (III), Met153 (IV) and Pro257–Asn261 (V) (residue numbering based on *P. polycephalum* cyt b_5R; Fig. 5). Lys122, Met153 and Pro257 are close to sites that are deleted in the proteins from lower eukaryotes compared with those from higher eukaryotes. The cause of the structural change at Ser106–Asp107 can be attributed to a difference in the hydrogen bonding of the residues. *P. polycephalum* cyt b_5R preserves a hydrogen bond between Ser106 O^{γ} and Glu109 N corresponding to the first of four hydrogen bonds (Ser98 O–Asp101 N, Asp99 $O^{\delta1}$–Gly71 N, Asp99 $O^{\delta2}$–Leu72 N and Asp101 $O^{\delta2}$–Ser98 N) in the human cyt b_5R; the other

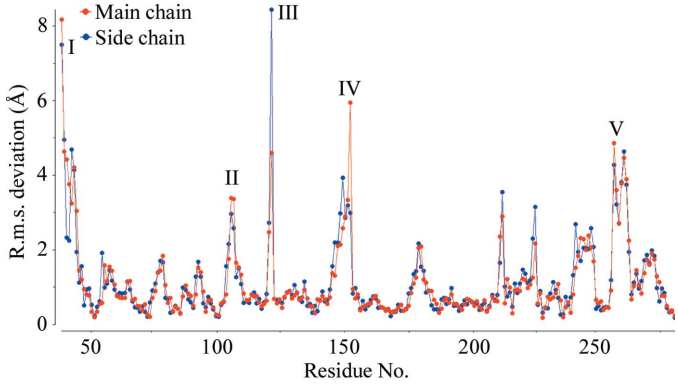

Figure 5
The r.m.s.d. in Å between common atoms from the corresponding residues of the *P. polycephalum* and human cyt b_5R proteins. The deviations for the main-chain and side-chain atoms are indicated in red and blue, respectively. Residue numbering is based on *P. polycephalum* cyt b_5R.

Table 3
Intramolecular ionic interactions of *P. polycephalum* and human cyt b_5R.

Positive	Negative	Distance (Å)
P. polycephalum cyt b_5R		
Arg40 N^{ε}	Asp76 $O^{\delta1}$	2.82
Arg40 $N^{\eta2}$	Asp76 $O^{\delta1}$	2.82
Arg68 N^{ε}	Asp114 $O^{\delta1}$	2.76
Arg68 $N^{\eta2}$	Asp114 $O^{\delta2}$	2.99
Arg201 $N^{\eta1}$	Glu195 $O^{\varepsilon2}$	2.76
Human cyt b_5R		
Arg49 $N^{\eta1}$	Glu131 $O^{\varepsilon1}$	2.95
Arg49 $N^{\eta2}$	Glu131 $O^{\varepsilon2}$	2.92
Arg57 $N^{\eta2}$	Glu131 $O^{\varepsilon1}$	2.68
Arg58 N^{ε}	Glu150 $O^{\varepsilon1}$	2.65
Arg60 N^{ε}	Asp106 $O^{\delta1}$	2.88
Arg60 $N^{\eta2}$	Asp106 $O^{\delta2}$	2.95
Lys153 N^{ζ}	Asp196 $O^{\delta2}$	2.68
Arg218 N^{ε}	Glu222 $O^{\varepsilon2}$	2.93
Arg218 $N^{\eta1}$	Glu212 $O^{\varepsilon2}$	2.91
Arg258 $N^{\eta2}$	Glu254 $O^{\varepsilon2}$	2.76

three hydrogen bonds are lost, resulting in a different conformation from the human cyt b_5R.

3.2. Structural features and thermostability of *P. polycephalum* and human cyt b_5R

The stability of a protein depends on its structure and is an effective indicator of the core structure of a protein. We examined the thermal stability of the *P. polycephalum* and human cyt b_5R proteins. The thermal denaturation of the proteins was monitored by DSC measurements at a scan rate of 1 K min^{-1} in 10 m*M* phosphate buffer pH 7.6 (Fig. 6). The *P. polycephalum* and human cyt b_5R protein solutions were turbid after heating, indicating that the heat denaturation of the proteins is not reversible under the conditions examined. Therefore, the data were not amenable to rigorous thermodynamic analysis. We then adopted the peak temperature on the DSC curve as the denaturation temperature (T_m). The *P. polycephalum* and human cyt b_5R proteins exhibited T_m values of 324.2 and 332.4 K, respectively; the denaturation temperature of the *P. polycephalum* cyt b_5R was 8.2 K lower than that at which human cyt b_5R denatures (Fig. 6).

Hydrogen bonds, ion pairs, accessible surface area (ASA) and cavity volume were examined in order to explore the structural features that resulted in the difference in the stabilities of the

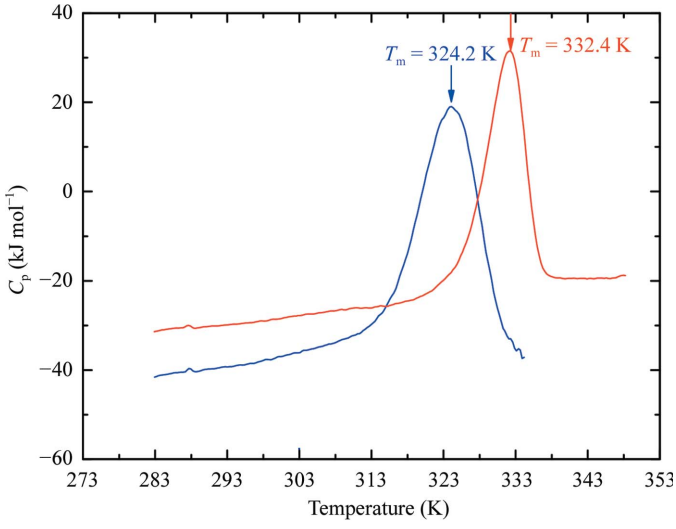

Figure 6
DSC curves for the *P. polycephalum* (blue) and human (red) cyt b_5R proteins.

Table 4
Estimation of the difference in stability of the *P. polycephalum* and human cyt b_5R proteins based on the structural information.

ΔASA represents the difference in the ASA between the native state and the denatured state of the enzymes. C/S and N/O represent nonpolar and polar atoms, respectively. $\Delta\Delta G$ represents the difference in ΔG between the *P. polycephalum* and human cyt b_5R proteins.

	P. polycephalum cyt b_5R	Human cyt b_5R
Hydrophobicity		
ΔASA (C/S) (Å^2)	15789.7	17749.4
ΔASA (N/O) (Å^2)	6465.0	6925.8
ΔG_{HP} (kJ mol^{-1})	11.7	301.8
$\Delta\Delta G_{HP}$ (kJ mol^{-1})	−290.0	—
Cavity volume		
Cavity (probe 1.4 Å) (Å^3)	218.8	69.4
ΔG_{CAV} (kJ mol^{-1})	−11.4	−3.6
$\Delta\Delta G_{CAV}$ (kJ mol^{-1})	−7.8	—
Hydrogen bonds†	193 (0.79)	227 (0.83)
Ion pairs†	5 (0.021)	10 (0.036)
Total No. of residues	243	275

† Values in parentheses are the number per amino-acid residue.

enzymes. The *P. polycephalum* and human cyt b_5R proteins consist of 243 and 275 amino-acid residues, respectively. The amino-acid compositions ratios were similar for the two proteins (Table 2). Residues that formed ion pairs within 3.0 Å are listed in Table 3. The total numbers of hydrogen bonds and ion pairs within 3.0 Å in the *P. polycephalum* and human cyt b_5R proteins were evaluated (Tables 3 and 4). The numbers of hydrogen bonds (0.79) and ion pairs (0.021) per amino-acid residue in *P. polycephalum* cyt b_5R are slightly lower than those (0.83 and 0.036, respectively) in human cyt b_5R.

Hydrophobic interactions are one of the important stabilizing forces of the folded conformation of proteins (Yutani *et al.*, 1977, 1987; Kellis *et al.*, 1988). The difference in the unfolding Gibbs energy change arising from hydrophobic effects ($\Delta\Delta G_{HP}$) between the *P. polycephalum* and human cyt b_5R proteins was estimated using the equation (Funahashi *et al.*, 2001)

$$\Delta\Delta G_{HP}\ (\mathrm{kJ\,mol^{-1}}) = 0.154\ (\mathrm{kJ\,mol^{-1}\,\AA^{-2}}) \times \Delta\Delta\mathrm{ASA}_{nonpolar}\ (\mathrm{\AA^2}) - 0.0254\ (\mathrm{kJ\,mol^{-1}\,\AA^{-2}}) \times \Delta\Delta\mathrm{ASA}_{polar}\ (\mathrm{\AA^2}),$$

where $\Delta\Delta\mathrm{ASA}_{nonpolar}$ and $\Delta\Delta\mathrm{ASA}_{polar}$ are the differences between the *P. polycephalum* and human cyt b_5R proteins in the change in the ASA of nonpolar and polar atoms, respectively, for all residues upon denaturation. The strength of the hydrophobic interactions (ΔG_{HP}) in *P. polycephalum* cyt b_5R was 290.0 kJ mol^{-1} lower than in human cyt b_5R (Table 4). This indicates that compared with human cyt b_5R, the weaker hydrophobic interactions in *P. polycephalum* cyt b_5R are the basis of the lower denaturation temperature observed for this protein.

The compact packing of amino-acid residues results in a small cavity volume in the internal portion of a protein (Eriksson *et al.*, 1992). The difference in the energy contribution to protein stability arising from cavity size (ΔG_{CAV}) between the *P. polycephalum* and human cyt b_5R proteins can be represented as (Funahashi *et al.*, 2001),

$$\Delta G_{CAV}\ (\mathrm{kJ\,mol^{-1}}) = -0.052\ (\mathrm{kJ\,mol^{-1}\,\AA^{-3}}) \times \Delta V\ (\mathrm{\AA^3}).$$

Compared with human cyt b_5R, the increase in the stabilization (ΔG_{CAV}) of *P. polycephalum* cyt b_5R arising from the change in the cavity volume was −7.8 kJ mol^{-1} (Table 4).

These results indicate that the difference in the hydrophobic interactions in the *P. polycephalum* and human cyt b_5R proteins was the primary factor underlying the lower denaturation temperature of *P. polycephalum* cyt b_5R, although differences in the internal packing of the two proteins contribute to the stability of the proteins.

References

Bando, S., Takano, T., Yubisui, T., Shirabe, K., Takeshita, M. & Nakagawa, A. (2004). *Acta Cryst.* D**60**, 1929–1934.
Bewley, M. C., Marohnic, C. C. & Barber, M. J. (2001). *Biochemistry*, **40**, 13574–13582.
Brünger, A. T., Adams, P. D., Clore, G. M., DeLano, W. L., Gros, P., Grosse-Kunstleve, R. W., Jiang, J.-S., Kuszewski, J., Nilges, M., Pannu, N. S., Read, R. J., Rice, L. M., Simonson, T. & Warren, G. L. (1998). *Acta Cryst.* D**54**, 905–921.
Collaborative Computational Project, Number 4 (1994). *Acta Cryst.* D**50**, 760–763.
Csukai, M., Murray, M. & Orr, E. (1994). *Eur. J. Biochem.* **219**, 441–448.
Davis, C. A., Crowley, L. J. & Barber, M. J. (2004). *Arch. Biochem. Biophys.* **431**, 233–244.
Emsley, P. & Cowtan, K. (2004). *Acta Cryst.* D**60**, 2126–32.
Eriksson, A. E., Baase, W. A., Zhang, X. J., Heinz, D. W., Blaber, M., Baldwin, E. P. & Matthews, B. W. (1992). *Science*, **255**, 178–183.
Fukuchi-Mizutani, M., Mizutani, M., Tanaka, Y., Kusumi, T. & Ohta, D. (1999). *Plant Physiol.* **119**, 353–362.
Funahashi, J., Takano, K. & Yutani, K. (2001). *Protein Eng.* **14**, 127–134.
Hildebrandt, A. & Estabrook, R. W. (1971). *Arch. Biochem. Biophys.* **143**, 66–79.
Hultquist, D. E. & Passon, P. G. (1971). *Nature New Biol.* **299**, 252–254.
Ikegami, T., Kameyama, E., Yamamoto S., Minami, Y. & Yubisui, T. (2007). In the press.
Iyanagi, T., Watanabe, S. & Anan, K. F. (1984). *Biochemistry*, **23**, 1418–1425.
Jones, S. J., Riddle, D. L., Pouzyrev, A. T., Velculescu, V. E., Hillier, L., Eddy, S. R., Stricklin, S. L., Baillie, D. L., Waterston, R. & Marra, M. A. (2001). *Genome Res.* **11**, 1346–1352.
Kamath, R. S., Fraser, A. G., Dong, Y., Poulin, G., Durbin, R., Gotta, M., Kanapin, A., Le Bot, N., Moreno, S., Sohrmann, M., Welchman, D. P., Zipperlen, P. & Ahringer, J. (2003). *Nature (London)*, **421**, 231–237.
Kellis, J. T., Nyberg, K., Sali, D. & Fersht, A. R. (1988). *Nature (London)*, **333**, 784–786.
Keyes, S. R. & Cinti, D. L. (1980). *J. Biol. Chem.* **255**, 11357–11364.
Klein, S. L., Strausberg, R. L., Wagner, L., Pontius, J., Clifton, S. W. & Richardson, P. (2002). *Dev. Dyn.* **225**, 384–391.
Laskowski, R. A., MacArthur, M. W., Moss, D. S. & Thornton, J. M. (1993). *J. Appl. Cryst.*, **26**, 283–291.
McPherson, A. (1999). *Crystallization of Biological Macromolecules.* New York: Cold Spring Harbor Laboratory Press.
Murshudov, G. N., Vagin, A. A. & Dodson, E. J. (1997). *Acta Cryst.* D**53**, 240–255.
Nishida, H., Inaka, K. & Miki, K. (1995). *FEBS Lett.* **361**, 97–100.
Nishida, H., Inaka, K., Yamanaka, M., Kaida, S., Kobayashi, K. & Miki, K. (1995). *Biochemistry*, **34**, 2763–2767.
Oshino, N., Imai, Y. & Sato, R. (1971). *J. Biochem.* **69**, 155–167.
Otwinowski, Z. & Minor, W. (1997). *Methods Enzymol.* **276**, 307–326.
Reddy, V. V. R., Kupfer, D. & Capsi, E. (1977). *J. Biol. Chem.* **252**, 2797–2801.
Rossmann, M. G. & Blow, D. M. (1962). *Acta Cryst.* **15**, 24–31.
Rossmann, M. G., Liljas, A., Branden, C. I. & Banaszak, L. J. (1975). *The Enzymes*, 3rd ed., edited by P. D. Boyer, Vol. 11, pp. 61–102. New York: Academic Press.
Rossmann, M. G., Moras, D. & Olsen, K. W. (1974). *Nature (London)*, **250**, 194–199.
Shirabe, K., Yubisui, T. & Takeshita, M. (1989). *Biochim. Biophys. Acta*, **1008**, 189–192.
Strittmatter, P. (1965). *J. Biol. Chem.* **240**, 4481–4487.
Yubisui, T., Miyata, T., Iwanaga, S., Tamura, S. & Takeshita, M. (1986). *J. Biochem.* **99**, 407–422.
Yutani, K., Ogasahara, K., Sugino, Y. & Matsusiro, A. (1977). *Nature (London)*, **267**, 274–275.
Yutani, K., Ogasahara, K., Tsujita, T. & Sugino, Y. (1987). *Proc. Natl Acad. Sci. USA*, **84**, 4441–4444.